# Journal of Materials Chemistry C



**PAPER** 

**View Article Online** 



Cite this: J. Mater. Chem. C, 2025, **13**. 954

Received 16th August 2024, Accepted 30th October 2024

DOI: 10.1039/d4tc03509g

rsc.li/materials-c

## Influence of shape on crystal structure and optical properties of heterocyclic conjugated molecules†

Elisa Guzmán, <sup>a</sup> Yu Yan, <sup>a</sup> Peter Müller, <sup>b</sup> Justin Amengual, <sup>c</sup> Mu-Ping Nieh <sup>d</sup> and Samuel W. Thomas III 1 \*\*

Organic optoelectronics are increasingly important due to their tunablilty, flexibility, and solution processability. Tuning optical properties of these materials as solids relies on the balance of weak noncovalent interactions that dictate crystal structure, but are difficult to predict. Our research aims to improve our understanding of how electrostatic interactions can direct and facilitate intramolecular interactions that dictate emergent properties of crystalline materials. This paper focuses on exploring how multi-fused thiophene ring systems that are popular in modern organic optoelectronic materials impact intramolecular interactions, while also investigating the role of molecular shape. In these examples, the shape of heterocyclic systems correlate with the crystal structures: while the bent heterocyclics show no discrete and discernable intramolecular interactions, those with bent shapes interact cofacially with one of the electron poor ArF pendants by twisting the arylene ethynylene backbone. Two of the control molecules, which bear non-fluorinated benzyl ester substituents, show intramolecular edge-face interactions, and several of these molecules show clear polymorphic behavior. These findings further our understanding of how discrete interactions can be altered not only by electrostatics, but also by shape, allowing for increasingly nuanced control over the crystal structures and optical properties of optoelectronic materials.

## Introduction

Conjugated organic materials present properties that are essential in numerous current and emerging applications, including luminescence for light emitting displays, 2-4 sensing, 2 and imaging, 5 as well as quasiparticle mobility for transistors and photovoltaics.<sup>6,7</sup> They also offer the boundless molecular design possibilities that organic chemistry brings. Through a combination of experimental and theoretical advances, these materials have realized remarkable progress in the performance of devices through an expanding structural diversity of materials—including both small molecules<sup>7-9</sup> and conjugated polymers<sup>10,11</sup>—that are, designed, synthesized, tested, and optimized. While we have sophisticated understanding and tools for pre-

dicting behavior of these materials in the gas phase or dilute

The approach of crystal engineering, which relies upon discrete non-covalent interactions to design and synthesize solid-state structures, 13,19 has become increasingly important in conjugated materials. While hydrogen bonding and halogen bonding involve structural elements that are not common features of most conjugated materials used in devices, chalcogen bonding and aromatic interactions feature structural units that are found in many conjugated materials. In the area of aromatic interactions, an electrostatic "polar-π" model, while

solution, solid-state behavior depends on many weak non-covalent interactions. 12,13 This especially includes non-specific and ubiquitous dispersion forces, which typically comprise the largest fraction<sup>14</sup> of the lattice energy and can result in numerous accessible low-energy crystal forms for the same molecule. Subtle differences in packing can yield substantial differences in both intramolecular torsion and the intermolecular aggregation between chromophores, which together control the key performance parameters in functional devices, such as charge mobility 15,16 or luminescence color and efficiency.<sup>17</sup> Unfortunately, even given the critical importance of solid-state packing of these materials, reliable approaches to controlling or predicting the packing18 of conjugated materials have lagged well behind other aspects of their development.

<sup>&</sup>lt;sup>a</sup> Department of Chemistry, Tufts University, 62 Talbot Ave, Medford, MA 02155, USA. E-mail: sam.thomas@tufts.edu

<sup>&</sup>lt;sup>b</sup> Department of Chemistry, Massachusetts Institute of Technology, Cambridge, MA 02139 USA

<sup>&</sup>lt;sup>c</sup> Polymer Program, Institute of Materials Science, University of Connecticut, 25 King Hill Road, Storrs, CT 06269-3136, USA

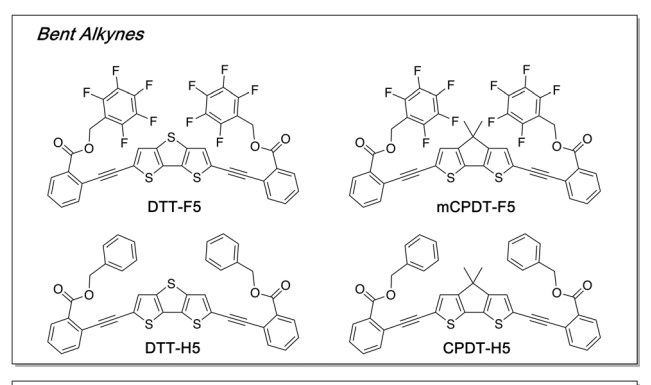
<sup>&</sup>lt;sup>d</sup> Department of Chemical & Biomolecular Engineering, University of Connecticut - Storrs, 97 North Eagleville Road, Unit 3136, Storrs,

<sup>†</sup> Electronic supplementary information (ESI) available. CCDC 2376091-2376096. For ESI and crystallographic data in CIF or other electronic format see DOI: https://doi.org/10.1039/d4tc03509g

insufficient to explain all observations and trends, can rationalize the trends observed. For example, edge-face interactions and slipped co-facial interactions are typical in the herringbone and bricklayer packing motifs of fused aromatic systems.<sup>20</sup> The cofacial interaction of non-fluorinated (ArH) and heavily fluorinated arenes (ArF) side chains with a chromophore is another commonly used type motif in crystal engineering of functional materials.21,22 Studies of optoelectronics<sup>23–25</sup> that focus on polymeric donoracceptor moieties either with 26-28 or without 29-35 thiophene units have shown non-covalent interactions of fluorinated rings impact crystal structure and properties of the devices. Other materials, including electrophosphors with metal centers,36 discotic liquid crystals<sup>37</sup> and fluorescent dyes<sup>38</sup> also use fluorination for directional non-covalent interactions.

In several papers, 39-47 we have described how fluorinated benzyl benzoates, when part of arylene-ethynylene (AE)-based conjugated materials, can undergo intermolecular and/or intramolecular pendant ArF-chromophore ArH cofacial stacking. The short tether of the linker to the benzylic ester pendant requires the AE backbone to twist out of coplanarity for the ArF-ArH interaction to occur. Having the triple bond with a low barrier of rotation between the chromophore and benzyl benzoate pendants allow for the molecules to access multiple configurations, as integrating molecular flexibility has been show to improve device performance. 48 Examining the F5 side chains (we note that fluorination has been shown to improve device performance)<sup>49</sup> and the H5 counterpart, which removes this directional non-covalent cofacial stacking interaction, can verify the impacts of the ArF-ArH interactions.

This specific interaction between the conjugated backbone and pendant groups (which are typically treated as ancillary segments of chemical space reserved for solubilizing chains) therefore increases band gap energies by reducing both intramolecular and intermolecular electronic coupling and can yield mechanofluorochomic materials<sup>39-41</sup> and phosphorescent solids.44 Our results45 of structure-property investigations of the side chain ArF-chromophore ArH interaction in this structural context point to electrostatic complementarity between the interacting rings determining whether they occur. To date we have almost exclusively focused on substituent effects on phenylene rings on the chromophore ArH rings. However, large and complex fused heteroaromatic systems, especially thio phene-containing fused multicyclic aromatic structures, are common in the best performing organic optoelectronics.<sup>50,51</sup> In a recent paper<sup>47</sup> we showed that the propensity for small monocyclic and fused bicyclic heterocycles to undergo ArFheterocycle chromophore stacking correlated with the magnitude of the computed electric field 3.2 Å away from the plane of the heterocycle in question. Building on this finding, the goal of this work is to determine whether pendant ArF-chromophore ArH non-covalent interactions can impact the crystal packing of larger thiophene-based fused heteroaromatic systems, for which simple predictions based on electronic substituent effects are not possible, and which are important structures found in p-type materials or as the donor segment of donor-acceptor materials.



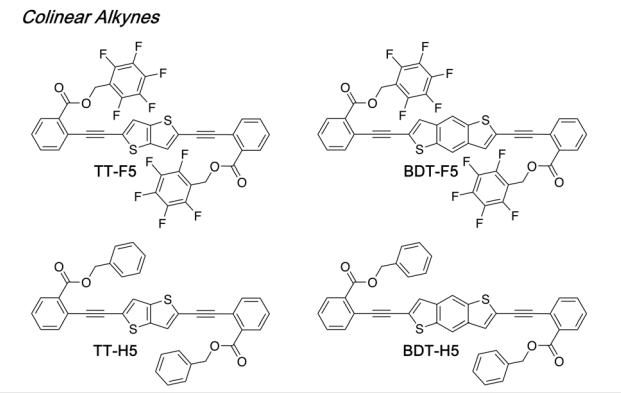


Chart 1 The eight new fused thienoarene-ethynylene molecules reported in this paper, organized by molecular shape. Each molecule comprises one of four central thienoarene cores and either perfluorobenzyl (F5) or benzyl (H5) pendants.

### Results and discussion

#### Experimental design and synthesis

Each of the eight molecules studied in this work (Chart 1) comprises a central thiophene-fused aromatic structure that is commonly found in modern optoelectronic materials,52-54 bound symmetrically to two o-benzyl benzoates through acetylene linkages. The pattern of these materials is similar to phenylene ethynylene materials we have previously investigated, in which the benzyl benzoate pendants occupy the termini of the chromophore. We prepared molecules with four different central aromatic cores, each of which is linked to either pentafluorobenzyl benzoate or unsubstituted benzyl benzoate pendants. Similar to previous work from our lab, the synthesis of these compounds followed a straightforward pathway. Acylation of either benzyl alcohol or pentafluorobenzyl alcohol with 2-iodobenzoic acid provided the aromatic pendants with iodinated phenyl groups. Subsequent Sonogashira coupling with trimethylsilylacetylene and deprotection with tetrabutylammonium fluoride gave the terminal benzyl ester units, which could undergo Sonogashira coupling with the dibromo derivatives of the target fused multicyclic arene core to yield the target compounds. The dibromides in these syntheses were either commercially available or previously reported.<sup>55</sup>

All four of the fused heteroaromatic cores-benzodithiophene, 56,57 thienothiophene,<sup>58</sup> dithienothiophene,<sup>59-61</sup> and cyclopentadienyl dithiophene 62,63-contain at least one fused thiophene ring and are

popular electronic donating heterocyclic systems in donoracceptor materials. 64,65 We can classify these molecules into two distinct classes of shapes, aspects of which we were also interested in exploring:

- (i) The ethynyl groups bound to tricyclic dithienothiophene (DTT) and cyclopentadienyldithiophene (mCPDT) cores are bent relative to the long molecular axis of the fused aromatic core. This feature results from the geometry of the five-member central ring of the fused tricyclic ring system. We note that our previously reported dimethylfluorene-based derivative (DMF-F5) shares this feature. 42
- (ii) The ethynyl groups share the long molecular axis of the fused aromatic core. This category includes thienothiophene (TT) and benzodithiophene (BDT) cores.

#### X-ray crystal structures

From the eight new molecules presented here, we were able to isolate X-ray quality single crystals for six of these compounds. In addition to TT-F5 and BDT-F5, this group of crystal structures comprise two pairs of fluorinated (F5) and unsubstituted (H5) analogs with the same aromatic cores (DTT and mCPDT), which allows for direct comparison of the influence of the pendant electronics on crystal structure. Fig. 1-3 show these crystal structures. Inspection of the crystal structures reveals several trends consistent across all six. One noteworthy example is the strong correlation between the conformations of the ester groups and the occurrence of intramolecular interactions between the aromatic pendant and the chromophore core. In each of the instances of the carbonyl group having anti relationship to the alkyne linker, a clear intramolecular interaction between the pendant arene and the main chain arene exists. Conversely, in all instances of the carbonyl group having a syn relationship to the alkyne linker, there are no intramolecular aromatic interactions, although intermolecular interactions of

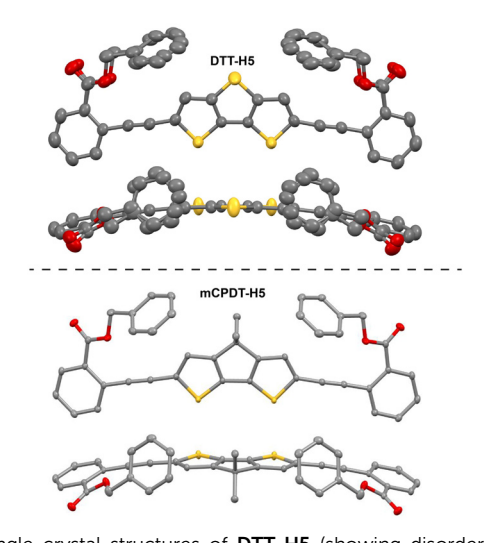


Fig. 1 Single crystal structures of DTT-H5 (showing disorder in benzyl ester substituents) and mCPDT-H5, highlighting their intramolecular edge-face interactions between phenyl pendants and tricyclic aromatic cores, as well as  $S \cdots \pi$  interactions. Hydrogen atoms omitted for clarity. Thermal ellipsoids shown at 50%.

the pendants and chromophores do still occur. We attribute this trend to the short three-atom tether between the aromatic pendant and the arylene ethynylene, combined with energetic favorability of coplanar conformations of the carboxylic ester groups with the arenes to which they are bound.

A second key trend is the nature of the arene-arene interactions that these molecules undergo for the linkers show anti conformations, which in this study all encompass molecules with ethynyl groups bent from the long axis of the tricyclic aromatic core. The carbonyl groups with unsubstituted benzyl pendants and anti conformations undergo edge-face interactions with the conjugated backbone. Both feature anti conformations of the two carbonyl groups, accompanied by intramolecular interactions between the faces of the phenyl pendants and C-H bonds of the central tricyclic unit: as shown in Fig. 1, DTT-H5 has a 3.40 Å distance between the 3-carbon of the DTT unit and the centroid of the phenyl substituent, while mCPDT-H5 shows a slightly elongated distance of 3.58 Å, which we attribute to steric buttressing of the geminal methyl groups on the cyclopentyl unit. In addition, these edge-face interactions are accompanied by roughly coplanar arylene ethynylene linkages (torsional angles of 9-11°). Overall these two molecules show nearly identical crystal packing motifs that feature numerous edge-face interactions of the pendant rings. These intramolecular edge-face interactions along the main chains of the chromophores coincide with coplanar arylene ethynylene linkages. Finally, the sulfur atoms of both the DTT and mCPDT unit point directly at the faces of another DTT or mCPDT unit, yielding chromophores arranged perpendicularly to each other, with S---centroid distances of 3.69 Å and 3.74 Å, respectively. These perpendicular arrangements, along with interactions between the edge of the pendant phenyl rings and the face of the tricyclic heterocyclic unit, appear to eliminate any obvious  $\pi$ -stacking of the chromophores.

Alternatively, the two fluorinated benzyl pendants with anti conformations undergo cofacial interactions with a main-chain arene, with closest atomic contacts of 3.47 Å and 3.45 Å for DTT-F5 and mCPDT-F5, and have twisted arylene-ethynylene backbones (torsional angles of 45-88°). We note that a molecule we reported previously (DMF-F5) that has the same molecular shape containing dimethylfluorene as a core instead of DTT or mCPDT shows the same "half-twisted" motif (see Fig. 2 for a comparison of these three crystal structures). Moreover, the intermolecular interactions of these three molecules also show strong similarity. For example, the F5 rings that cause AE twisting through intramolecular cofacial interaction also undergo intermolecular cofacial interactions with the coplanar half of the  $\pi$ -conjugated main chain of a nearby molecule. Furthermore, the F5 rings that do not interact intramolecularly are swung out to the side, stacking with the twisted benzoate ring of a nearby AE chromophore, with the tricyclic arene of this second molecule in the pointing in the opposite direction of the first. As a result of the fluorinated rings not fully shielding the faces of the conjugated backbones through co-facial interactions, inter-chromophore aggregation via  $\pi$ -stacking between the main chains of these three molecules is readily obvious.

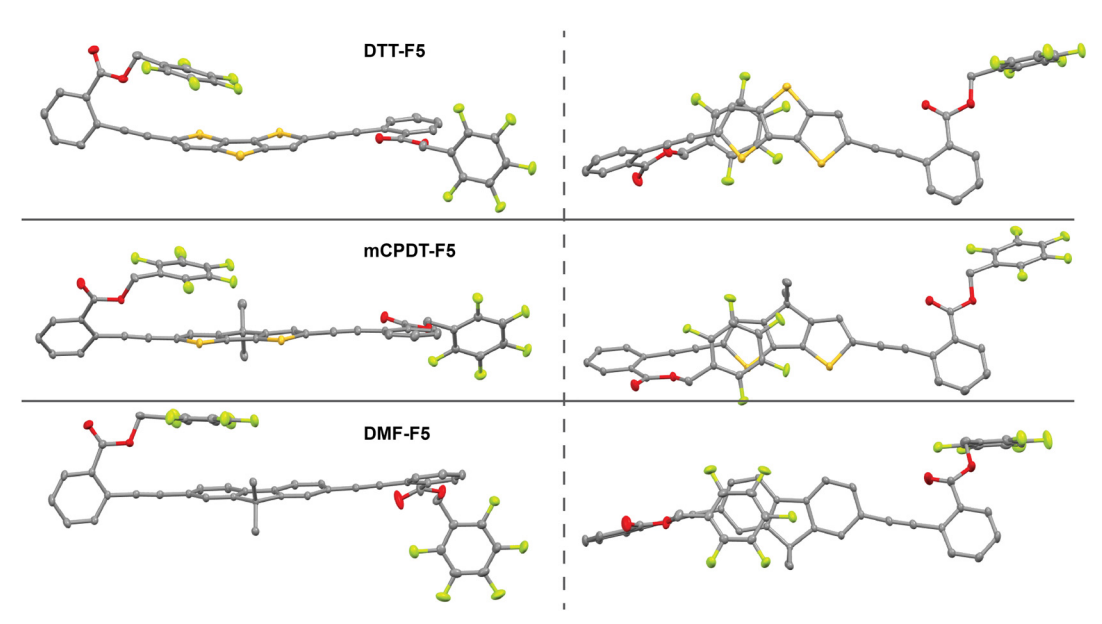


Fig. 2 Edge-on (left) and top-down (right) views of the crystal structures of DTT-F5, mCPDT-F5, and the previously reported DMF-F5, 42 all of which have bent tricyclic fused aromatic cores and share "half-twisted" crystal structures. Hydrogen atoms omitted for clarity. All thermal ellipsoids shown at 50%.

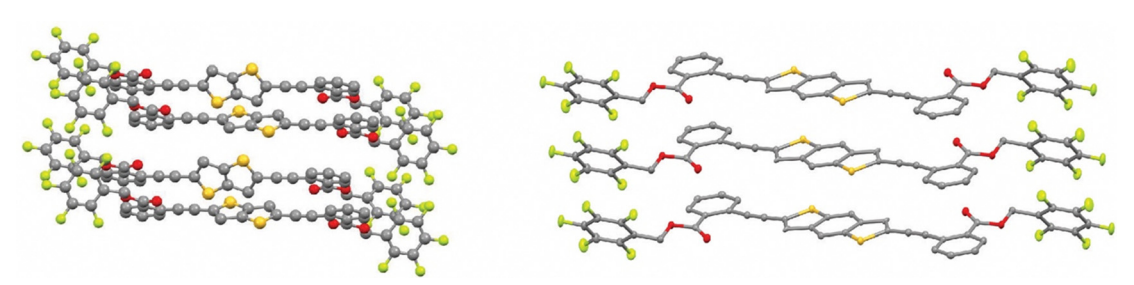


Fig. 3 X-ray crystal structures of fluorinated derivatives of the linear AE chromophores, which lack pendant ArF-chromophore ArH interactions. TT-F5 (left) shows intermolecular S-π interactions, while **BDT-F5** (right) shows slipped stacking. Hydrogen atoms have been removed for clarity, and thermal ellipsoids are shown at 50%

Finally, the crystal structures of the fluorinated derivatives of the linear chromophores-TT-F5 and BDT-F5-feature high degrees of segregation between the fluorinated benzyl pendants and the conjugated backbones (Fig. 3). Neither feature pendant ArF-chromophore ArH interactions of any kind, and present intermolecular F.··F interactions as the only short contacts of the fluorinated rings. For TT-F5 the conjugated backbones feature similar S- $\pi$  interactions as in DTT-H5 and mCPDT-H5 with S---centroid distances of 3.18 Å. Each sulfur atom and each face of a thiophene participates in these edge-face interactions, resulting in stacks of these interactions propagating in two perpendicular directions within the crystal structure. The appearance of S- $\pi$  interactions in molecular balances and protein crystal structures has previously been attributed to increasingly favorable dispersion interactions of the polarizable sulfur atom. 66,67 The conjugated chromophores of TT-F5 are slightly twisted, with torsional angles of approximately 37° between the arylene rings. The conjugated chromophores of BDT-F5 do not feature S- $\pi$  interactions, instead presenting

intermolecular slipped stacks of the planar (torsional angles of 2-4°) arylene-ethynylene units and, separately, the fluorinated pendants, each with 3.5–3.6 Å inter-ring distances. While we have not been able to isolate X-ray quality crystals of the non-fluorinated H5 derivatives of TT and BDT, the fact that the fluorinated analogs do not show intramolecular pendant ArF-chromophore ArH interactions makes this crystallographic comparison less important, especially considering the similar solid-state optical spectra of the F5 and H5 derivatives of each of these two pairs of molecules.

#### Optical properties

To understand the influence of chemical structure on optical properties, we measured the steady-state absorbance and fluorescence spectra of these molecules in CH2Cl2 (Fig. 4). Several trends emerge in these spectra. One is that the spectral positions of the F5/H5 pairs of molecules do not change substantially for the same conjugated backbone. The fluorescence spectra of the F5 analogs are slightly red-shifted from

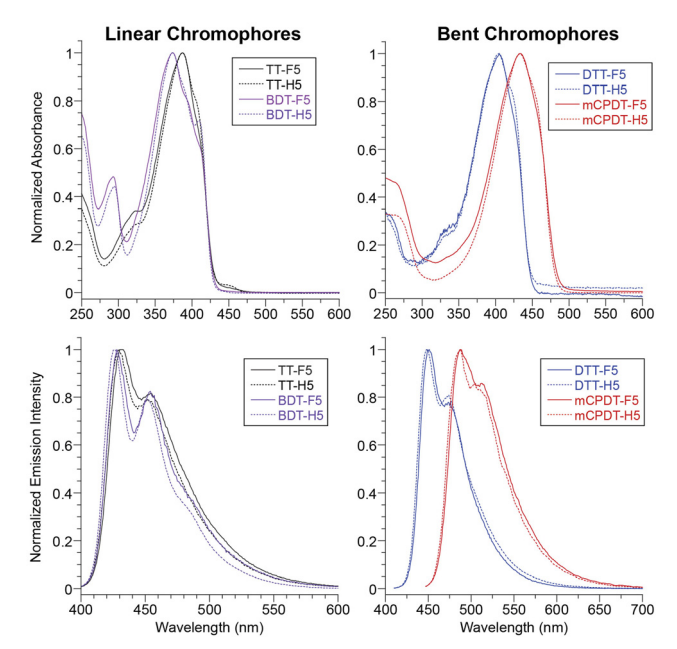


Fig. 4 Solution phase absorbance (top) and fluorescence (bottom) spectra of the eight molecules from Chart 1 in dilute CH2Cl2 solution.

their H5 counterparts by 2-4 nm, which we attribute to the inductive effects of the fluorine atoms making the benzoate rings slightly better electron acceptors.<sup>68</sup> These four chromophores span a modest range of wavelengths in solution, with  $\lambda_{\text{max}}$  values at 389 nm (TT) to 430 nm (mCPDT) for absorbance spectra, and 430 nm to 490 nm for fluorescence spectra. Spectral positions correlate with extent of  $\pi$ -conjugation as expected. The extinction coefficients of all molecules at their lowest energy  $\lambda_{max}$  wavelengths are in the expected range of 30 000-60 000 M<sup>-1</sup> cm<sup>-1</sup>, and all molecules are reasonably fluorescent in solution, with  $\Phi_{\rm F}$  values between 0.3 and 0.5 (Table 1).

All energy minimized geometries of these molecules in density functional theory calculations, using the B3LYP functional and the 6-31G (d,p) basis set, show highly coplanar relationships between the central heterocycles and the conjugated benzoate rings. Calculations and results are shown in the ESI† starting at page S39. The lowest energy computed excited state for all eight molecules upon geometry optimization were allowed by the computed oscillator strengths, and all involved

Table 1 Optical properties of the molecules from Chart 1

	$\lambda_{ ext{max,abs}}^{a}$ (nm)	$E_{\text{onset,abs}}$ (eV)	$\varepsilon$ (M <sup>-1</sup> cm <sup>-1</sup> )	$\begin{matrix} \lambda_{\text{max, emis}}{}^a \\ \text{(nm)} \end{matrix}$	$\Phi_{ m F}$	τ (ns)
TT-H5	389	2.90	50 000	430	0.45	0.47
TT-F5	389	2.88	41000	432	0.43	0.46
BDT-H5	372	2.90	57 000	427	0.46	0.69
BDT-F5	373	2.89	36 000	428	0.43	0.37
DTT-H5	405	2.78	59 000	451	0.50	0.68
DTT-F5	405	2.77	52 000	450	0.52	0.70
mCPDT-H5	430	2.58	57 000	490	0.35	0.71
mCPDT-F5	430	2.56	62 000	490	0.33	0.71

<sup>&</sup>lt;sup>a</sup> Solution data collected in CH<sub>2</sub>Cl<sub>2</sub>.

only the HOMO and LUMO orbitals. Consistent with our experimental observations, the computed excited state energies of fluorinated and non-fluorinated derivatives of each pair of conjugated heterocycles were nearly identical, differing within each pair by no more than 0.02 eV. Moreover, the trend in computed excited state energies of these molecules follows that observed experimentally, with the BDT and TT derivatives having the highest excited state energies, and the mCPDT derivatives having the lowest.

The absorbance and emission spectra of these molecules as drop-cast or spun-cast thin films are substantially red-shifted, in all cases, from their dilute solution-phase samples, with direct comparisons shown in Fig. S11-S15 (ESI†). This is consistent with our observation that all the crystal structures in this work show interchromophore aggregation between the main AE chains, and contrasts strongly with many molecules we have previously reported, in which the fluoroarene pendants block interchromophore aggregation. For comparing the spectra of these solid samples, we heated these films to 100 °C in an effort to bias their structures to lower energy polymorphs, as we noted different colors of solids under different solvent evaporation conditions. While these molecules share some of the same structural features as those in our prior reports, that this insulation from aggregation is missing in these examples highlights the challenge of predicting solid state band gaps of solids.69 Further complicating the analysis of these data are the prevalence of polymorphs in these structures, which in some cases we have been able to correlate with single crystal X-ray structures using wide angle powder X-ray diffraction analysis of solid samples prepared with different procedures (vide infra).

Beyond these general features of the solid-state spectra, some differentiation does appear when comparing the bent class of AE materials-DTT and mCPDT-which correlates with their crystal structures. While the excitation spectra of these solids do not show any clear trends, the  $\lambda_{max}$  of luminescence emission spectra of drop-cast, annealed films of the F5 derivatives of these molecules are blue-shifted modestly from the corresponding H5 analogs, by 25-30 nm, even though their solution-phase spectra are nearly identical, Fig. S12 and S15 (ESI†) respectively. This is consistent with the difference in crystal structures: in these two F5 derivatives, one fluoroarene stacks with the main chain and twists an arylene-ethynylene linkage, while the H5 analogs have highly coplanar backbones reinforced by intramolecular edge face interactions. However, the spectroscopic impact of a twist in the AE backbone is substantially smaller than prior systems we have studied<sup>45,47</sup> that comprise a central terephthalate ring with two conjugated ArH rings as termini, in which highly twisted molecules can show noticeably larger bandgaps than those observed in solution for the same molecules. TD-DFT results reflect this mitigated spectroscopic effect, with the lowest energy excited states of the hydrogenated and fluorinated individual molecules in their crystallographically determined geometries not showing any significant difference in excited state energies, while the calculated oscillator strengths of the twisted

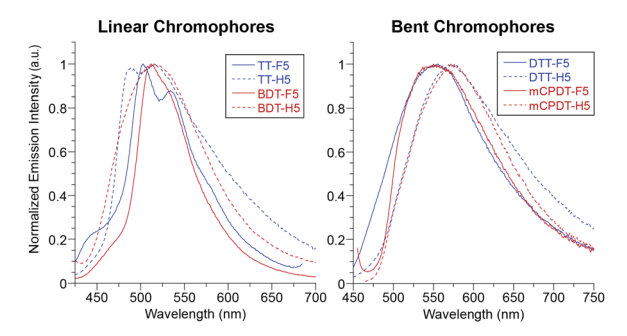


Fig. 5 Fluorescence emission spectra of thin films of these eight molecules prepared by spin casting and after annealing to 100 °C.

fluorinated derivatives are substantially smaller than those for the planar hydrogenated derivatives.

Similarly, all four solids in the linear TT and BDT class show luminescence that is substantially red-shifted from these molecules in dilute solution (Fig. 5). In contrast, however, spun-cast thin films with linear TT and BDT backbones did not show substantially different spectral positions of luminescence spectra when comparing the F5 and H5 derivatives. This observation is consistent with the two crystal structures we have in this class-TT-F5 and BDT-F5-which show intermolecular co-facial interactions between conjugated carbon atoms on the benzoate rings with distances between 3.4-3.6 Å. As the fluorinated pendants do not offer protection against aggregation or substantial twisting of the conjugated backbones of TT-F5 and BDT-F5, we would not expect annealed solids of these molecules and their H5 analogs solid to show substantially different band gaps. This is also reflected in the TD-DFT computed lowest excited state energies for individual molecules of TT-F5 and BDT-F5 in their crystallographic determined geometries,

which show no more than a 0.2 eV difference in excited state energy compared to the computed excited state of their energyminimized geometries in solution.

#### **Polymorphism**

In an effort to elucidate the impact of polymorphism on the solid-state properties of these samples, we attempted to correlate luminescence properties, experimental powder X-ray diffraction patterns, and simulated powder patterns from single crystal structures (Fig. 6). With the exception of TT-H5, for which we were able to separate yellow and orange polymorphs by hand, we isolated polymorphs, when possible, by screening various solvents, temperatures, and cooling rates, while observing the extent to which solids with different visible colors formed. More details on isolating the polymorphs can be found on pages S3-S4. Both of the bent arenes DTT-H5 and mCPDT-H5 showed clear evidence of polymorph formation, as solids with different colors and different luminescence spectra could be isolated. The summary of these spectra is tabulated in Table S1 (ESI†), along with the melting point analysis based on the DSCs seen in Fig. S16-S23 (ESI†). DTT-H5 yielded red and orange polymorphic solids with the higher-melting orange polymorph yielding a powder pattern matching well to that simulated from the X-ray crystal structure of **DTT-H5** in Fig. 2, considering instrumental smearing. For mCPDT-H5, for which red and orange solids could be isolated, the powder pattern of an orange polymorph matched the simulated powder pattern from the crystal structure in Fig. 2, also considering instrumental smearing. Pictures of the isolated polymorphic solids, together with the matching experimental and simulated powder XRD results, are presented in Fig. 6. Neither the mCPDT-H5 (Fig. S23, ESI†) nor the DTT-H5 (Fig. S19, ESI†) exhibit a repeatable melting point of the isolated solid, but the isolated

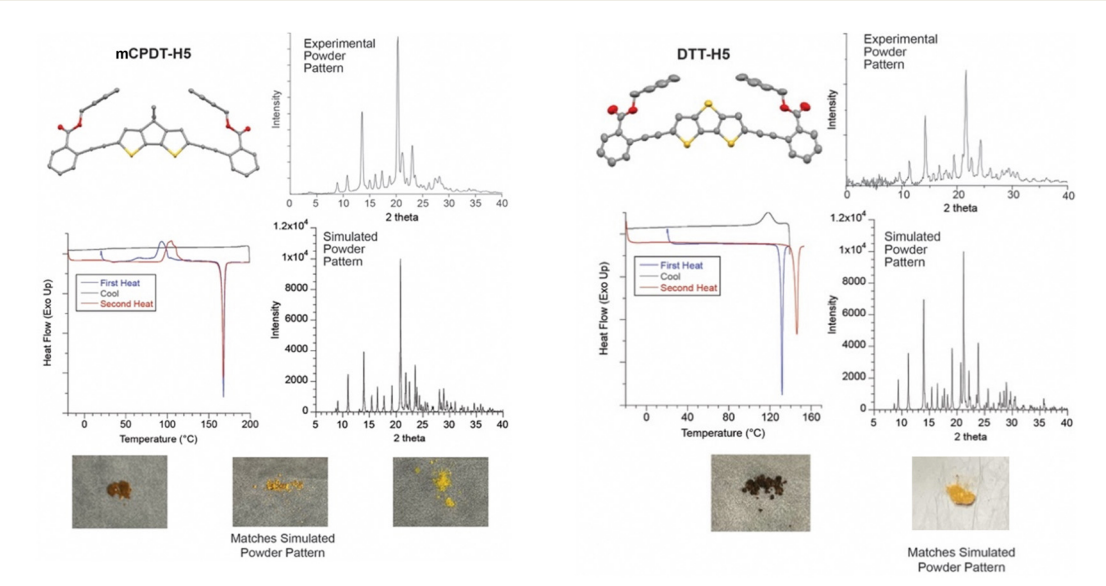


Fig. 6 Agreement of experimental powder pattern for one polymorph for mCPDT-H5 (left) and DTT-H5 (right) with powder pattern simulated from single crystal X-ray structure for each. Differential scanning calorimetry for mCPDT-H5 shows cold crystallization followed by a consistent melting point of one polymorph, while DTT-H5 shows transition of one polymorph into another upon melting and fusing

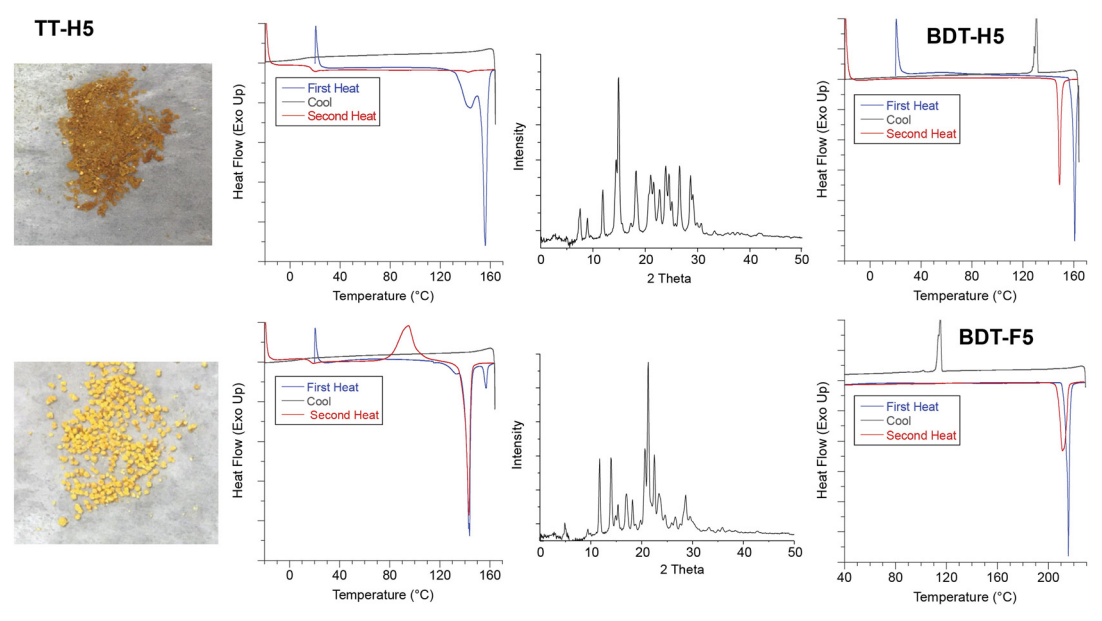


Fig. 7 Left: Manually separated orange (top) and yellow (bottom) polymorphs of TT-H5, with DSC indicating the yellow polymorph is more stable, as it reforms selectively upon melting and fusing. Right: DSC traces showing polymorph formation upon melting and cooling of BDT derivatives.

DTT-H5 polymorph shows that recrystallization by melting accesses a different polymorph.

Several of the linear chromophores also display polymorphism (Fig. 7). While we were unable to detect any polymorphism of TT-F5, we could isolate two polymorphs of TT-H5 by hand. They display different melting points by DSC (Fig. S17, ESI,† yellow at 143 °C, and orange at 156–157 °C), and significantly different powder X-ray diffraction patterns, indicating different crystal structures for these two samples. The other linear chromophore BDT also showed evidence of polymorphic solids in both the H5 and F5 compounds. BDT-H5 polymorphs could not be separated by solution-based recrystallization, as only a yellow solid (mp  $\sim$  160 °C) formed (Fig. S20, ESI†). However, based on DSC and visual analysis, a different, orange-colored polymorph (mp 149 °C) formed selectively during recrystallization of the melted yellow solid. BDT-F5 also showed polymorphic behavior according to the DSC traces (Fig. S21, ESI†).

### Conclusions

This paper describes new conjugated arylene ethynylene molecules with four different, fused thienoarenes commonly used in organic optoelectronic materials, in order to understand the impact of the electronics of benzyl ester side chains on solid-state packing and optical properties. The two bent tricyclic chromophores-dithienothiophene and dithieno-cyclopentadiene-show "half-twisted" arylene ethynylenes, with one of the two fluoroarene pendants undergoing pendant ArF-chromophore ArH stacking with the chromophore intramolecularly. Interestingly, this motif is shared with a similarly bent, fluorene-based chromophore. Bent molecules with unsubstituted phenyl pendants show electrostatically favorable edgeface intramolecular interactions. On the other hand, the linear

chromophores-thienothiophene and benzodithiophene-lack any intramolecular stacking interactions. The optical properties of these solids correlate with these crystal packing motifs, although the trends are modest for these molecules, as they do not have strong donor-acceptor character along the conjugated backbone, and all undergo some degree of interchromophore aggregation. Finally, several of these molecules show readily separated polymorphs.

Overall, these observations suggest that in addition to the electronic character of the potentially interacting arenes, the shapes of the molecules play essential roles in determining whether discrete interactions of the aromatic rings occur in the crystal structures. While trends that connect chemical structure to crystal packing in these molecules are not as well defined as some of our previous studies, which used a central terephthalate ring, they do extend the utility that the ArF-ArH cofacial stacking interaction can have in dictating intramolecular conformation of conjugated systems, and also open new questions as to why certain heterocyclic systems do show these interactions, and others do not. More generally, these results reveal the possibilities for using discrete, directional interactions of aromatic rings for rational control over the conformations of conjugated molecules containing thiophene-rich fused heterocycles popular in high performance organic electronic materials.

## Data availability

Crystallographic data for the TT-F5, BDT-F5, DTT-F5, DTT-H5, mCPDT-F5, and mCPDT-H5 has been deposited at the CCDC under accession numbers 2376091-2376096. Other data supporting this article have been included as part of the ESI.†

## Conflicts of interest

There are no conflicts to declare.

## Acknowledgements

This work was supported by the U.S. Department of Energy, Basic Energy Sciences, through award DE-SC0016423. E. G. was supported by a National Science Foundation Graduate Research Fellowship.

## Notes and references

- 1 N. Sun, Y. Han, W. Huang, M. Xu, J. Wang, X. An, J. Lin and W. Huang, Adv. Mater., 2024, 36, 2309779.
- 2 J. Peng, L. Hou, D. Liu, Z. Zhao, J. Zhang, Z. Qiu and B. Z. Tang, ACS Appl. Opt. Mater., 2024, 2, 15-27.
- 3 M. Hancharova, K. Mazur, K. Halicka and D. Zając, J. Polym. Res., 2022, 29, 417.
- 4 W. Xiong, C. Zhang, Y. Fang, M. Peng and W. Sun, Polymers, 2023, 15, 98.
- 5 J. Wei, Y. Liu, J. Yu, L. Chen, M. Luo, L. Yang, P. Li, S. Li and X.-H. Zhang, Small, 2021, 17, 2103127.
- 6 A. G. S. Al-Azzawi, S. B. Aziz, E. M. A. Dannoun, A. Iraqi, M. M. Nofal, A. R. Murad and A. M. Hussein, Polymers, 2023, **15**, 164.
- 7 D. Molina, M. J. Álvaro-Martins and Á. Sastre-Santos, J. Mater. Chem. C, 2021, 9, 16078-16109.
- 8 O. Ostroverkhova, Chem. Rev., 2016, 116, 13279-13412.
- 9 H. Wang, C. Zhao, Z. Burešová, F. Bureš and J. Liu, J. Mater. Chem. A, 2023, 11, 3753-3770.
- 10 S. Topal, G. Suna, P. Ulukan, E. Sezer and T. Ozturk, Electrochim. Acta, 2021, 392, 139020.
- 11 S. Topal, O. Savlug Ipek, E. Sezer and T. Ozturk, Chem. Eng. J., 2022, 434, 133868.
- 12 J. W. Hwang, P. Li and K. D. Shimizu, Org. Biomol. Chem., 2017, 15, 1554-1564.
- 13 A. Haque, K. M. Alenezi, M. S. Khan, W.-Y. Wong and P. R. Raithby, Chem. Soc. Rev., 2023, 52, 454-472.
- 14 S. Parida, S. K. Patra and S. Mishra, ChemPhysChem., 2022, 23, e202200361.
- 15 Z.-Y. Wang, L. Di Virgilio, Z.-F. Yao, Z.-D. Yu, X.-Y. Wang, Y.-Y. Zhou, Q.-Y. Li, Y. Lu, L. Zou, H. I. Wang, X.-Y. Wang, J.-Y. Wang and J. Pei, Angew. Chem., Int. Ed., 2021, 60, 20483-20488.
- 16 Y.-W. Huang, Y.-C. Lin, Y.-S. Wu, Y.-T. Wong, M.-Y. Kuo, W.-C. Chen and C.-C. Chueh, Ind. Eng. Chem. Res., 2020, 59, 9105-9115.
- 17 B. Huang, W.-C. Chen, Z. Li, J. Zhang, W. Zhao, Y. Feng, B. Z. Tang and C.-S. Lee, Angew. Chem., Int. Ed., 2018, 57,
- 18 C. Sutton, C. Risko and J.-L. Brédas, Chem. Mater., 2016, 28,
- 19 A. S. Novikov, Crystals, 2022, 12, 246.

- 20 C. Wang, D. Hashizume, M. Nakano, T. Ogaki, H. Takenaka, K. Kawabata and K. Takimiya, Chem. Sci., 2020, 11, 1573-1580.
- 21 R. Ragni, A. Punzi, F. Babudri and G. M. Farinola, Eur. J. Org. Chem., 2018, 3500-3519.
- 22 A. Y. Sosorev, V. A. Trukhanov, D. R. Maslennikov, O. V. Borshchev, R. A. Polyakov, M. S. Skorotetcky, N. M. Surin, M. S. Kazantsev, D. I. Dominskiy, V. A. Tafeenko, S. A. Ponomarenko and D. Y. Paraschuk, ACS Appl. Mater. Interfaces, 2020, 12, 9507-9519.
- 23 I. P. Koskin, C. S. Becker, A. A. Sonina, V. A. Trukhanov, N. A. Shumilov, A. D. Kuimov, Y. S. Zhuravleva, Y. O. Kiseleva, I. K. Shundrina, P. S. Sherin, D. Y. Paraschuk and M. S. Kazantsev, Adv. Funct. Mater., 2021, 31, 2104638.
- 24 X. Zhou, S. Pang, B. Wu, J. Zhou, H. Tang, K. Lin, Z. Xie, C. Duan, F. Huang and Y. Cao, ACS Appl. Energy Mater., 2022, 5, 7710-7718.
- 25 M. Barłóg, I. Kulai, X. Ji, N. Bhuvanesh, S. Dey, E. P. Sliwinski, H. S. Bazzi, L. Fang and M. Al-Hashimi, Org. Chem. Front., 2019, 6, 780-790.
- 26 Q. Zhang, L. Yan, X. Jiao, Z. Peng, S. Liu, J. J. Rech, E. Klump, H. Ade, F. So and W. You, Chem. Mater., 2017, 29, 5990-6002.
- 27 J. Chen, L. Wang, J. Yang, K. Yang, M. A. Uddin, Y. Tang, X. Zhou, Q. Liao, J. Yu, B. Liu, H. Y. Woo and X. Guo, Macromolecules, 2019, 52, 341-353.
- 28 J.-W. Ha, J. B. Park, H. J. Park and D.-H. Hwang, Polymers, 2020, 12, 2121.
- 29 J. Lee, M. Jang, S. M. Lee, D. Yoo, T. J. Shin, J. H. Oh and C. Yang, ACS Appl. Mater. Interfaces, 2014, 6, 20390-20399.
- 30 M. Chen, Z. Zhang, W. Li, J. Cai, J. Yu, E. L. K. Spooner, R. C. Kilbride, D. Li, B. Du, R. S. Gurney, D. Liu, W. Tang, D. G. Lidzey and T. Wang, Sci. China: Chem., 2019, 62, 1221-1229.
- 31 M. Chen, D. Liu, W. Li, R. S. Gurney, D. Li, J. Cai, E. L. K. Spooner, R. C. Kilbride, J. D. McGettrick, T. M. Watson, Z. Li, R. A. L. Jones, D. G. Lidzey and T. Wang, ACS Appl. Mater. Interfaces, 2019, 11, 26194-26203.
- 32 S. Wood, J.-H. Kim, D.-H. Hwang and J.-S. Kim, Chem. Mater., 2015, 27, 4196-4204.
- 33 J. Cai, H. Wang, X. Zhang, W. Li, D. Li, Y. Mao, B. Du, M. Chen, Y. Zhuang, D. Liu, H.-L. Qin, Y. Zhao, J. A. Smith, R. C. Kilbride, A. J. Parnell, R. A. L. Jones, D. G. Lidzey and T. Wang, J. Mater. Chem. A, 2020, 8, 4230-4238.
- 34 S. Dai, J. Zhou, S. Chandrabose, Y. Shi, G. Han, K. Chen, J. Xin, K. Liu, Z. Chen, Z. Xie, W. Ma, Y. Yi, L. Jiang, J. M. Hodgkiss and X. Zhan, Adv. Mater., 2020, 32, 2000645.
- 35 H. S. Kim, S. Rasool, W. S. Shin, C. E. Song and D.-H. Hwang, ACS Appl. Mater. Interfaces, 2020, 12, 50638-50647.
- 36 L. He, L. Duan, J. Qiao, D. Zhang, G. Dong, L. Wang and Y. Qiu, Synth. Met., 2013, 166, 52-56.
- 37 H.-M. Pan, J. He, W.-H. Yu, P. Hu, B.-Q. Wang, K.-Q. Zhao and B. Donnio, J. Mater. Chem. C, 2023, 11, 14695-14704.
- 38 K. Funabiki, K. Yamada, Y. Arisawa, A. Watanabe, T. Agou, Y. Kubota, T. Inuzuka, Y. Miwa, T. Udagawa and S. Kutsumizu, J. Org. Chem., 2022, 87, 11751-11765.

- 39 S. A. Sharber, K.-C. Shih, A. Mann, F. Frausto, T. E. Haas, M.-P. Nieh and S. W. Thomas, Chem. Sci., 2018, 9, 5415-5426.
- 40 S. A. Sharber and S. W. Thomas, Chem. Mater., 2020, 32, 5785-5801.
- 41 S. A. Sharber, A. Mann, K.-C. Shih, W. J. Mullin, M.-P. Nieh and S. W. Thomas, 3rd, J. Mater. Chem. C, 2019, 7, 8316-8324.
- 42 W. J. Mullin, R. H. Pawle, S. A. Sharber, P. Müller and S. W. Thomas, J. Mater. Chem. C, 2019, 7, 1198-1207.
- 43 S. A. Sharber and S. W. Thomas III, Chem. Eur. J., 2018, 24, 16987-16991.
- 44 W. J. Mullin, H. Qin, T. Mani, P. Müller, M. J. Panzer and S. W. Thomas, Chem. Commun., 2020, 56, 6854-6857.
- 45 S. A. Sharber, R. N. Baral, F. Frausto, T. E. Haas, P. Müller and S. W. Thomas III, J. Am. Chem. Soc., 2017, 139, 5164-5174.
- 46 S. W. Thomas III, R. H. Pawle and Z. C. Smith, J. Photochem. Photobiol., A, 2016, 322-323, 119-128.
- 47 W. J. Mullin, P. Müller, A. J. Schaefer, E. Guzman, S. E. Wheeler and S. W. Thomas Iii, J. Mater. Chem. C. 2022, 10, 11199-11210.
- 48 T. Lei, J.-Y. Wang and J. Pei, Chem. Mater., 2014, 26, 594-603.
- 49 Q. Zhang, M. A. Kelly, N. Bauer and W. You, Acc. Chem. Res., 2017, 50, 2401-2409.
- 50 O. Sahin, M. E. Cinar, E. Tekin, S. P. Mucur, S. Topal, G. Suna, M. S. Eroglu and T. Ozturk, ChemistrySelect, 2017, 2, 2889–2894.
- 51 G. Turkoglu, M. E. Cinar and T. Ozturk, Top. Curr. Chem., 2017, 375, 84.
- 52 Z. Feng, Z. Cheng, H. Jin and P. Lu, J. Mater. Chem. C, 2022, 10, 4497-4520.
- 53 C. Yang, S. Zhang and J. Hou, Aggregate, 2022, 3, e111.
- 54 K. Feng, H. Guo, H. Sun and X. Guo, Acc. Chem. Res., 2021, **54**, 3804-3817.

- 55 N. Ferri, N. Algethami, A. Vezzoli, S. Sangtarash, M. McLaughlin, H. Sadeghi, C. J. Lambert, R. J. Nichols and S. J. Higgins, Angew. Chem., Int. Ed., 2019, 58, 16583-16589.
- 56 M. Shavez and A. N. Panda, J. Phys. Chem. A, 2021, 125, 9852-9864.
- 57 H. Yue, M. Guo, S. Ming, H. Du, J. Zhao and J. Zhang, Colloids Surf., A, 2024, 684, 133094.
- 58 Y. Xue, Z. Xue, W. Zhang, W. Zhang, S. Chen, K. Lin and J. Xu, J. Electroanal. Chem., 2019, 834, 150-160.
- 59 O. S. Ipek, S. Topal and T. Ozturk, Dyes Pigm., 2021, 192, 109458.
- 60 R. Ali and R. Siddiqui, RSC Adv., 2022, 12, 36073-36102.
- 61 B. B. Carbas and H. B. Yildiz, Eur. Polym. J., 2024, 204, 112700.
- 62 C. S. Sarap, Y. Singh, J. M. Lane and N. Rai, Sci. Rep., 2023, 13, 21587.
- 63 N. Casanova, S. Shankar S, M. J. Gómez-Escalonilla, P. de la Cruz, R. Singhal, G. D. Sharma and F. Langa, ACS Appl. Energy Mater., 2023, 6, 12052-12063.
- 64 P. Xie, T. Liu, J. Sun and J. Yang, Adv. Funct. Mater., 2022, 32, 2200843.
- 65 M. Seifrid, G. N. M. Reddy, B. F. Chmelka and G. C. Bazan, Nat. Rev. Mater., 2020, 5, 910-930.
- 66 J. Hwang, P. Li, M. D. Smith, C. E. Warden, D. A. Sirianni, E. C. Vik, J. M. Maier, C. J. Yehl, C. D. Sherrill and K. D. Shimizu, J. Am. Chem. Soc., 2018, 140, 13301-13307.
- 67 A. L. Ringer, A. Senenko and C. D. Sherrill, *Protein Sci.*, 2007, 16, 2216-2223.
- 68 R. H. Pawle, A. Agarwal, S. Malveira, Z. C. Smith and S. W. Thomas, III, Macromolecules, 2014, 47, 2250-2256.
- 69 Z.-F. Yao, J.-Y. Wang and J. Pei, Prog. Polym. Sci., 2023, 136, 101626.